Characterization of ultrasound elevation beamwidth artifacts for prostate brachytherapy needle insertion

Mohammad Peikari,[a)] Thomas Kuriran Chen, Andras Lasso, Tamas Heffter, and Gabor Fichtinger
Laboratory for Percutaneous Surgery (Perk), School of Computing, Queen's University, Kingston, Ontario K7L 3N6, Canada

Everette C. Burdette
Acoustic MedSystems, 208 Burwash Avenue, Savoy, Illinois 61874

(Received 19 July 2011; revised 21 November 2011; accepted for publication 22 November 2011; published 20 December 2011)

Purpose: Ultrasound elevation beamwidth leads to image artifacts and uncertainties in localizing objects (such as a surgical needle) in ultrasound images. The authors examined the clinical significance of errors caused by elevation beamwidth artifacts and imaging parameters in needle insertion procedures.
Methods: Beveled prostate brachytherapy needles were inserted through all holes of a grid template under real-time transrectal ultrasound (TRUS) guidance. The needle tip position as indicated by the TRUS image was compared to their observed physical location. A new device was developed to measure the ultrasound elevation beamwidth.
Results: Imaging parameters of the TRUS scanner have direct impact on the localization error ranging from 0.5 up to 4 mm. The smallest localization error was observed laterally close to the center of the grid template and axially within the beam's focal zone. Largest localization error occurs laterally around both sides of the grid template and axially within the beam's far field. The authors also found that the localization errors vary with both lateral and elevation offsets.
Conclusions: The authors found properly adjusting the TRUS imaging settings to lower the ultrasound gain and power effectively minimized the appearance of elevation beamwidth artifacts and in turn reduced the localization errors of the needle tip. [DOI: 10.1118/1.3669488]

Key words: ultrasound imaging, main lobe, side lobe, localization error, brachytherapy

I. INTRODUCTION

I.A. Clinical significance and background

Prostate cancer is the second leading cause of cancer death in men in the United States and one of the most common cancers in North America.[1] Prostate brachytherapy is an effective treatment for early-stage prostate cancer. There are two methods of brachytherapy widely used: low dose rate (LDR) and high dose rate (HDR). LDR involves permanent implantation of small radioactive seeds into the prostate gland under real-time transrectal ultrasound (TRUS) guidance to the cancer, whereas HDR involves placing thin catheters, needles, or other applicators in the tumor to deliver a relatively intense therapeutic dose of radiation under TRUS guidance. The success of both the procedures depends on an accurate seed/catheter placement. Errors in implant locations could result in dosimetric degradation of the treatment.

The patient is placed on the lithotomy position and TRUS probe is placed inside his rectum, as shown in Fig. 1. Transperineal implant needles/catheters are inserted through the guide holes of the template in planned locations. The needle tip position is tracked in transversal plane of a TRUS. When inserted to the correct cancer site in the prostate, the radioactive seeds are deposited (in LDR)[2,3] or therapeutic radiation sources are delivered using and afterloading device to the tumor (in HDR).

I.B. Elevation beamwidth artifacts

Ultrasound (US) imaging is one of the most widely used modalities in medical diagnosis and interventions. US is acoustic energy transmitted in the form of waves through the medium having a frequency above the human hearing range (more than 20 MHz). Image artifacts are commonly encountered in medical ultrasound images. It has been discussed in the literature that US may contain certain types of artifacts caused by the beam orthogonal to both the axial and lateral beam axes, the main beam thickness, and the side lobes. The artifacts may lead to a misinterpretation of the true tissue structure.[4] The target application of this research is prostate brachytherapy (Fig. 1).

The main beam thickness of TRUS is a unique problem of TRUS-guided brachytherapy because the needles are inserted perpendicular to the transverse TRUS beam. Hence, the nonuniform main beam thickness causes error in localizing needle tips which in turn may lead to inaccurate needle placements and dose delivery. In addition, the off-axis side lobe echoes could worsen the amount of localization error by showing the off-axis objects in incorrect location in the TRUS images. Although technically, the sagittal plane of the TRUS probe could be used to guide parallel needles to the correct depth, but not all the currently used TRUS probes

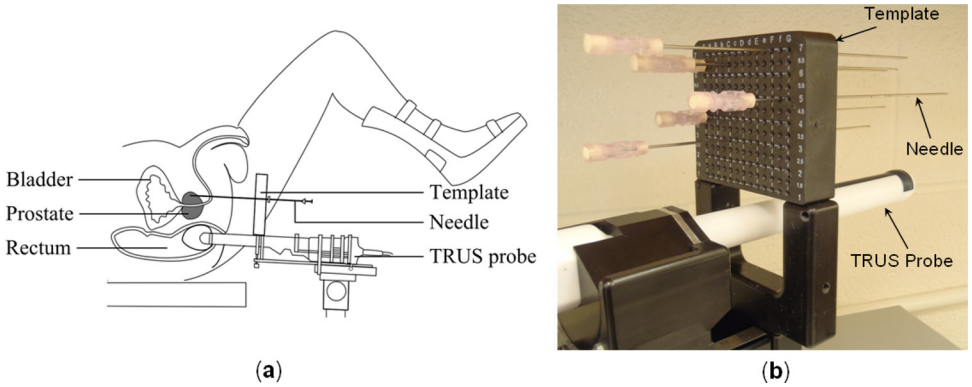

FIG. 1. (a) A schematic showing prostate brachytherapy procedure. (b) Implanting needles inserted through grid template holes.

have the sagittal plane transducer. Furthermore, in practice many of the physicians avoid using the US sagittal images and only rely on the images taken from transverse plane. The objective of this work is to study the clinical relevance of the needle tip placement error in transverse plane in presence of the two main sources of errors, the main and side lobe artifacts of the TRUS. Accurate needle tip localization is an important step toward radiation therapy quality improvements because implant geometry highly affects the dose distribution in brachytherapy procedures.[5]

The US image is created by interpreting the intensities of the reflected echoes when intersected with an object tissue located at a known distance to the transducer. It is generally assumed that the US image is of zero thickness which contradicts the fact that the US beam can only be mechanically focused at a depth resulting in a finite, nonuniform elevation beamwidth. The quality of the US image along the beam's elevation axis is defined by the *elevation resolution* (Fig. 2), in which the US device assumes that all the received echoes originate from structures located precisely on the central line of the US beam[4,6] as depicted in Fig. 2(b).

Figures 2(b) and 2(c) show the cross-section of a focused TRUS beam pattern and its corresponding B-mode and A-mode echoes. In an A-mode imaging, a simple transducer scans a line through the medium with the echoes presented as function of depth. Similarly, in a B-mode imaging, a linear array of transducers simultaneously scan a plane from the medium with echoes presented as a two-dimensional (2D) image. Returning echoes are generated after TRUS beam intersects with reflecting materials located within the beam's boundary. The first three reflected echoes correspond to the reflecting objects (A-C) located at the same axial distance. Since the strength of the TRUS beam energy is maximum near the central line of the sound wave and decreases elevationally,[4,6] the maximum echo amplitude corresponds to the reflecting point A and the minimum amplitude echo corresponds to point C. The TRUS energy intensity degrades as the beam travels through the medium farther away from its source (transducer). Hence, the overall intensities of the reflected echoes from points D and F decrease as shown in Fig. 2(c).

Echoes from the same axial distance and lateral position of the TRUS beam arrives to the transducer at the same time. TRUS device sums all the simultaneously received echoes and interpret their values as a single object located on the TRUS central beam line. As a result, echoes receiving from any other objects not located on the TRUS central beam line will be considered to be from the objects located on the central beam line, shown as point F in Fig. 2(b). Therefore, reflectors located elevationally farther from the beam central line do not appear at their true position.

Transducer side lobes consist of multiple low energy sound beams emitted off-axis from the main TRUS lobe that produce image artifacts due to error in positioning the returning echo as shown in Fig. 3. Although the TRUS beam pattern is generally considered to be fairly coherent within the near field, in reality, the beam diverges quickly without focusing.[6–11] Acoustic lenses are therefore used to improve

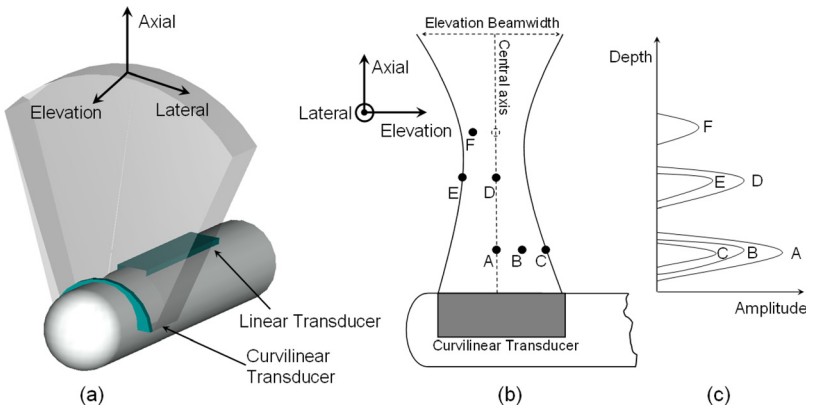

FIG. 2. (a) TRUS beam pattern in *axial*, *lateral*, and *elevation* axes. (b) and (c) Beam pattern of a B-mode and A-mode TRUS with corresponding point reflectors.

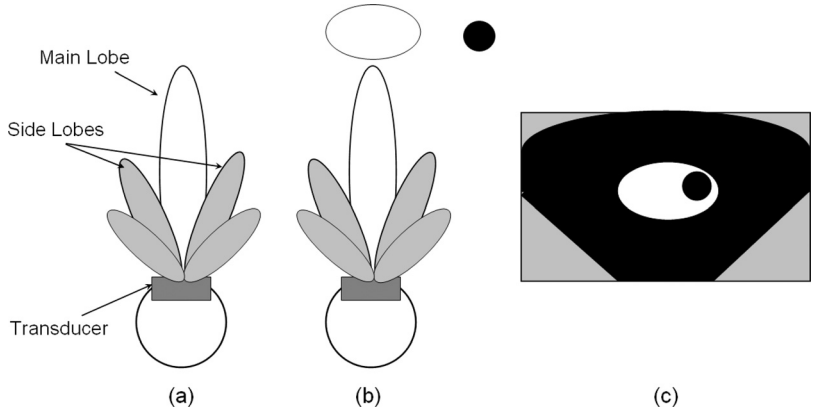

FIG. 3. (a) Two-dimensional representation of the main and side lobe beams. (b) Diagram showing the off-axis side lobe energies encountering two objects. (c) The TRUS device assumes that the returning echoes from the off-axis side lobes came from the main beam and misplaces the structure.

the lateral and elevational image quality by focusing the sound wave at a specific axial depth.[6,7,12] The beam pattern, therefore, consist of a *main lobe* which looks like an inverted cone with its apex located at a known distance (focal depth) from the transducer face. In addition to the main lobe of sound, unwanted parts of the TRUS beam are also produced which occur outside of the main beam [Fig. 3(a)]. Theoretical calculations of the side lobe intensities suggest that the energy of the side lobe beams are at most one-hundredth of the main TRUS beam (20 dB lower).[10] This level of intensity is however sufficient to produce enough echoes (side lobe artifacts) from the strong reflectors located off the main beam.[6] Side lobe artifacts appear as a series of parallel low-intensity lines at regular intervals[6,10,13] near curved and highly specular reflector surfaces.[10]

The TRUS device assumes that the depth at which an echo is displayed is proportional to the time it takes for the echo to leave the transducer, reflect off the reflective surface, and return to the transducer. Side lobe artifacts occur when the off-axis beams interact with highly reflective acoustic surfaces. Hence, the returning echoes to the transducer are recorded to be along the path of the main TRUS beam as shown in Figs. 3(b) and 3(c).

I.C. Prior art in elevation beamwidth characterization

Goldstein and Madrazo[4] was the first to examine the effects of the TRUS elevation beamwidth on the images by using an inclined plane. He observed the elevation beamwidth artifacts on different human organ geometries using longitudinal and transverse scans of the tissues. Richard[14] later tried to measure the beam thickness using several parallel inclined surfaces at 45° located 15 mm below each other to capture many elevation beamwidth artifacts in one single image for low frequency probes. Skolnick[15] compared both the scan plane and elevation beamwidth artifacts by sweeping a linear array US probe oriented 90° and 45° to his experimental phantoms. He used two phantoms for his experiments, one with multiple filaments located 1 cm apart from each other in a vertical row, and the other one with an inclined surface to the US beam. He obtained close measurements of the elevation beamwidth artifacts when experimenting with both of the mentioned phantoms.

Liang and Kurtz[10] first reported the effects and importance of the side lobe artifacts on the US images. He illustrated the genesis of these artifacts and provided clinical examples of the commonly visualized side lobe artifacts. Barthez *et al.*[16] reproduced the side lobe artifacts *in vitro* using different US transducers and tried to recognize these artifacts *in vivo*. He observed the side lobe effects when imaging a phantom composed of a water bath, a metallic wire, and a wooden tongue depressor. He imaged the phantom using all sorts of US probes (linear array, curved linear array, vector array, and sector mechanical transducer). There also have been several works to improve the US image quality and eliminate the off-axis US energies by implementing different adoptive beam forming methods on radio frequency data.[17–21]

A recent study conducted by Siebert *et al.*[22] quantitatively measured the visibility and accuracy of implant needle tips in transversal and sagittal TRUS planes. The absolute position of the needle tip was measured with respect to a marker system parallel to the TRUS probe. They reported detection errors between 0.8 and 3.1 mm for both sagittal and transversal viewing planes. It is worth to mention that in their research they did not consider the effects of different imaging parameters. The parameters could highly influence the observation and measurement of the needle tip in TRUS images.

II. MATERIALS AND METHODS

II.A. TRUS beamwidth calculation principles

In this work, we refer the TRUS elevation beamwidth artifact as a combination of the main lobe thickness and the low-intensity side lobes. We also refer the TRUS beamwidth artifact depth to be the axial distance from the TRUS transducer face to the middle of the bright artifact on the images. We measure the TRUS beamwidth using the same approach originally proposed by Goldstein and Madrazo.[4] According to his approach, if we image a 45° oriented diffusive surface to the TRUS beam, the TRUS beamwidth is the thickness of the resultant artifact on the TRUS image.

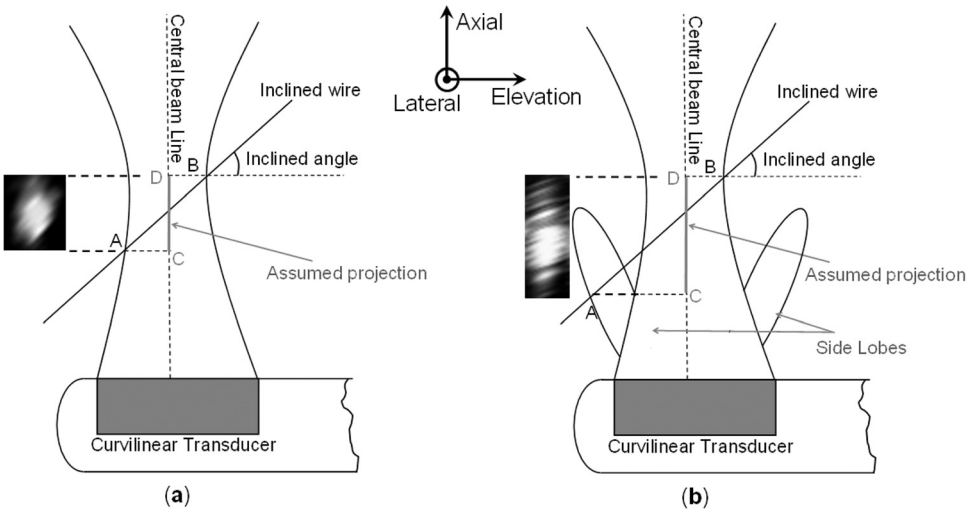

FIG. 4. (a) Ultrasound beamwidth measurement principle in presence of the main lobe only. (b) Ultrasound beamwidth measurement principle in presence of the main lobe and side lobe energies.

Figure 4(a) shows the cross-section of a TRUS main beam intersected with a diffusive inclined wire/surface along the elevation axis of the beam. As the TRUS beam propagates through the coupling medium, it first intersects with point A (closest point to the transducer) on the inclined diffusive material. The inclined wire and the TRUS beam have to maintain 45° with respect to each other. The last point with which the TRUS beam intersects with is point B (farthest point to the transducer). The sound echoes from the inclined wire return to the transducer. On the other hand, the TRUS device sums all the simultaneously returned echoes assuming they are actually from the reflectors located on the central beam axis. Hence, the line AB would be displayed as line CD by the TRUS device, as shown in Fig. 4(a) with its thickness approximately representing the TRUS beamwidth.

If there are side lobe energies present around the TRUS main lobe, the corresponding returned echoes to the transducer are considered to be the echoes returned after intersecting the TRUS main lobe to the reflecting materials. Hence, the same concept applies to categorizing the returned echoes by the TRUS device as explained before with the exception that the TRUS device would include a thicker bright artifact in the images because the side lobe energies were the first to intersect with the inclined diffusive material. The side lobe generated echoes will have lesser intensities since the side lobe energy levels are much lesser than the main lobe energies as shown in Fig. 4(b).

II.B. Wire-Bridge phantom

We have previously developed a device (the *TRUS-Bridge* phantom) to measure and quantify the elevation beamwidth of TRUS probes.[12,23] The TRUS-Bridge phantom had an inclined surface oriented 45° angle to the TRUS main beam emitted from the transducer. A rubber membrane was used to cover the inclined surface since the latex material can make a good reflector in water. In this work, we used a modified version of the TRUS-Bridge phantom, where we replaced the rubber membrane with nylon wires (*Wire-Bridge* phantom). We used multiple nylon wires in place of the rubber material to ensure the measurements are not influenced by the thickness of the rubber membrane. Thirteen wires were placed at the same lateral position as the template grid holes, as shown in Fig. 5(b).

The Wire-Bridge phantom was specifically designed to accommodate any standard commercial brachytherapy stepper. The phantom was made of high-strength, industry-grade thermoplastic (acrylonitrile butadiene styrene) and equipped with supporting side walls and screw holes to be rigidly

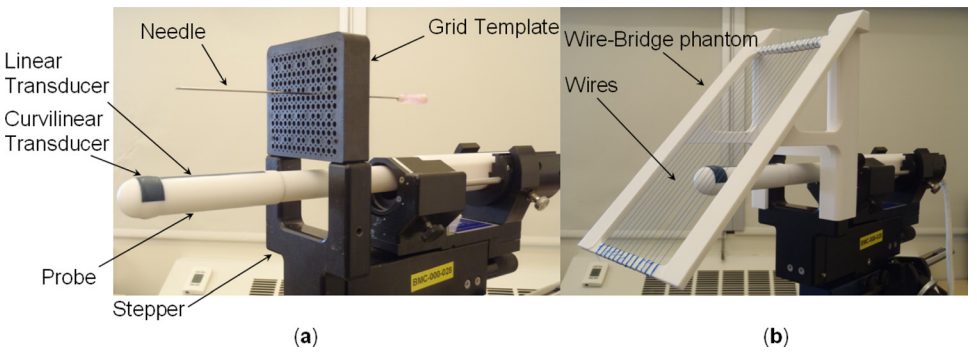

FIG. 5. (a) Different parts of the clinical TRUS device. (b) The Wire-Bridge phantom on a clinical TRUS stepper.

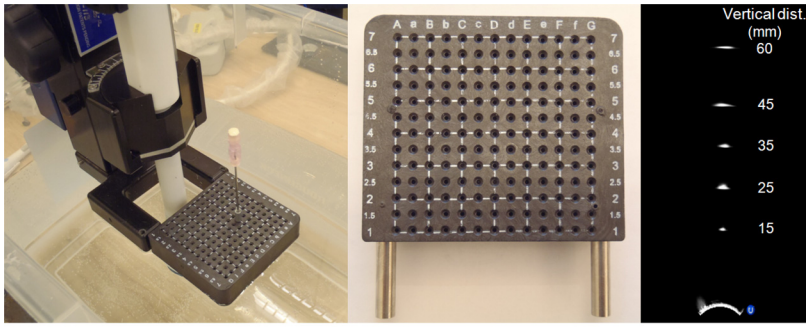

FIG. 6. (a) Needle insertion experimental setup. TRUS probe and needles are deep into a glycerol–water bath. (b) Standard grid template used to guide needle insertion in brachytherapy procedures. (c) Needle tip appearance and their vertical distances to the TRUS transducer at gain = 0%, dynamic range = 15 dB, and power = −7.

affixed onto the stepper on the template holder, which ensures the geometric accuracy of the inclined wires.

II.C. Needle localization error measurements

We calculated the needle localization error by first measuring the boundary of the TRUS beam where the first needle tip reflections are starting to appear. The brachytherapy needles are inserted and fixed through the grid template holes. The TRUS probe is then moved back and forth along the elevation axis of the beam until the inserted needle tip reflection starts to appear in the TRUS images. We then recorded the digital encoder values of the brachytherapy stepper position at which the needle tips are first observed in the TRUS images along the axial axis of the TRUS beam for each inserted needle.

The observed needle positions are then compared to a reference point to find the relative convergence and divergence of the beam with respect to a starting point. The reference point in our experiments is the point at which the first inserted needle reflection appears in a vertical column [corresponding to the row number 1 on the grid template guide, Fig. 6(b)]. This gives us an estimate of the needle tip localization offset with respect to the TRUS beam shape. We measure this offset at each template hole where the needle is inserted (both laterally and axially). The depths of other observed inserted needle tips at other axial positions corresponding to the exact position of the template grid holes are subtracted from the reference point to give an estimate of the needle offset with respect to the reference needle. Hence, the beamwidth relationship between every two inserted needles is defined as follow:

$$B(j) = 2(N(i) - N(j)) + B(i),$$

where i and j are the two inserted needle indexes being compared along axial depths; $N(i)$ and $N(j)$ are the needle insertion depths for the two needles i and j, respectively; and $B(i)$ and $B(j)$ are the beam thicknesses at the corresponding i and j axial depths, respectively, as shown in Fig. 7.

When there are side lobes, the needle tips intersect with these energies sooner than they intersect with the main lobe. As mentioned before, the TRUS device assumes that the echoes from side lobe energies are from the reflectors intersected with the main lobe and it positions these echoes within the main beam echoes. Hence, in this case the needle tip reflections appear sooner than when intersecting with the main lobe as depicted in Fig. 7(b).

II.D. Hardware configurations

There are three parts of a TRUS system to consider: a TRUS probe, a stepper, and a grid template guide as shown

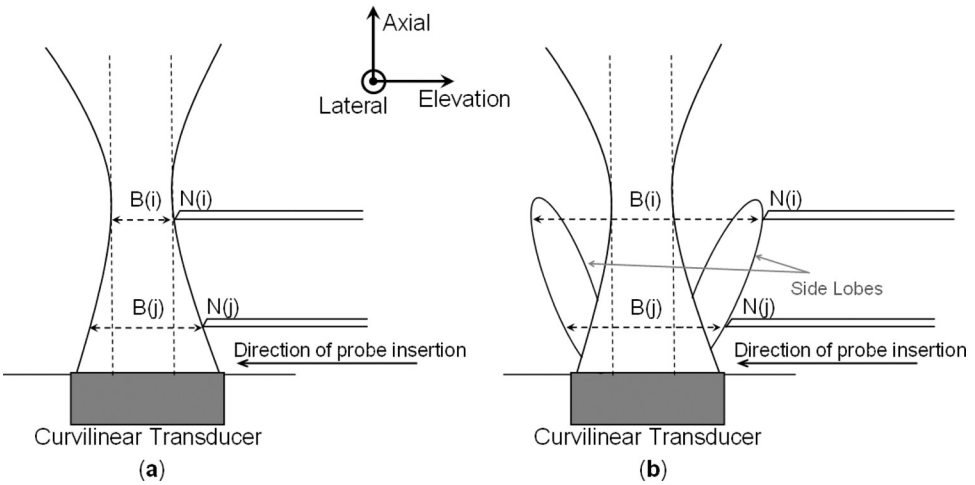

FIG. 7. (a) Needle offset measurement principle in presence of main lobe only. (b) Needle offset measurement principle in presence of main lobe and side lobe energies.

in Fig. 5(a). The TRUS probe can move in and out (along the elevation axis of the beam) of the patient's rectum allowing the physician to observe and track the prostate in live TRUS imagery during the procedure. The grid template on the TRUS stepper guides the physician during the needle insertion process. The stepper allows the TRUS probe always to move perpendicularly to the grid template and the TRUS beam. Images were acquired using the SonixTouch device (Ultrasonix, Richmond, British Columbia, Canada) and the transverse transducer type was BPC8-4/10. The needle used in our experiments was a spinal needle with Quincke type point from Becton Dickinson & Co. (size: 1.27 mm diameter and 15.24 cm length).

II.E. Experimental setup

In order to examine the effects of the TRUS imaging parameters on the beam pattern and localization error, we performed a series of needle insertion tests for 27 combinations of TRUS gain (0%, 50%, and 100%), dynamic range (15, 50, and 100 dB), and power (0, − 4, and − 7). A total of 169 needles inserted with the guidance of grid template were mounted on the brachytherapy stepper for each of the 27 combinations. We examined a wide variety of cases to have an estimate of localization errors for different lateral positions of the beam. Table I shows the combinations of different TRUS imaging settings used to acquire images in our experiment.

II.E.1. TRUS beamwidth measurement

We used the Wire-Bridge phantom to measure beam profiles at lateral locations that exactly correspond to the columns of the template grid holes. The phantom contains 13 parallel inclined wires positioned 5 mm apart according to the template hole lateral positions. Several TRUS images were acquired with different imaging parameters (gain, power, and dynamic range) at the central frequency of 6 MHz (one of the frequencies at which the brachytherapy procedures are commonly being operated), as shown in Fig. 8(b). The phantom was replaced by the grid template and fixed rigidly using screws to the template holder. TRUS images were acquired in a bath of distilled water and 7% glycerol by weight [Fig. 8(a)]. The glycerol-doped medium provides a speed of sound of 1540 m/s at a temperature of 20 °C which matches the speed of sound in human tissues.[4,24]

II.E.2. Needle tip localization analysis

We used the grid template to guide needle insertion in our experiments. The template contains a matrix of 13×13 dimension of holes. The size of the grid matrix is 60 mm by 60 mm and there is a 5 mm gap between its rows and columns. The vertical distance from the upper edge of the 2D-array of the TRUS probe to the first row of guide holes [labeled with 1 in Fig. 6(b)] was 10 mm. Use of the template grid helped to ensure that the needles are inserted perpendicularly to the TRUS beam along its elevation axis.

The TRUS probe was moved back and forth along the elevation axis of the beam until the first needle tip reflection appeared in the TRUS images; the stepper position was then recorded for that elevational depth, as shown, in Fig. 6(a). Needle tip reflections appeared as bright spots in the TRUS images as shown in Fig. 6(c). This needle tip measurement was repeated for all 169 holes of the grid template to estimate the localization error for all possible needle insertions during a brachytherapy procedure. Different imaging parameters (gain, power, and dynamic range) were used for these experiments at central frequency of 6 MHz to see the effect of these parameters on observing the location of the needle tips in the TRUS images.

II.E.3. Comparison between beam profile and needle tip profile

In order to compare the TRUS beam profile and the needle tip profile, we conducted several experiments with similar imaging settings (gain, power, and dynamic range). For the beam profile measurements, we kept the device's dynamic range and power at a constant value and set the gain to three values to cover the whole range of possible gain values (from low to high gain). We did not conduct the beam profiling experiments for different dynamic range and power values since we had observed that different settings of these two parameters did not change the overall measurement of the beamwidth. However, the needle tip profiling experiments were conducted with all possible combinations of the imaging parameters, since the needle tip localization offset measurements with different imaging parameters were the main goal of this research work. The results of the experiments for all imaging parameters were combined by taking the mean and standard deviation of the values at similar settings.

II.E.4. Side lobe extraction

The inclined wires of the phantom cover the entire elevation axis of the beam. Hence, the inclined wires can cover both TRUS main and side lobes. A bright spot with highest intensity appears in the images when the main TRUS beam intersects with the inclined fishing wires. In addition, a group

TABLE I. Combinations of different TRUS imaging settings used in our experiments.

Gain (%)	0									50									100								
Dynamic range (dB)	15			50			100			15			50			100			15			50			100		
Power	0	−4	−7	0	−4	−7	0	−4	−7	0	−4	−7	0	−4	−7	0	−4	−7	0	−4	−7	0	−4	−7	0	−4	−7

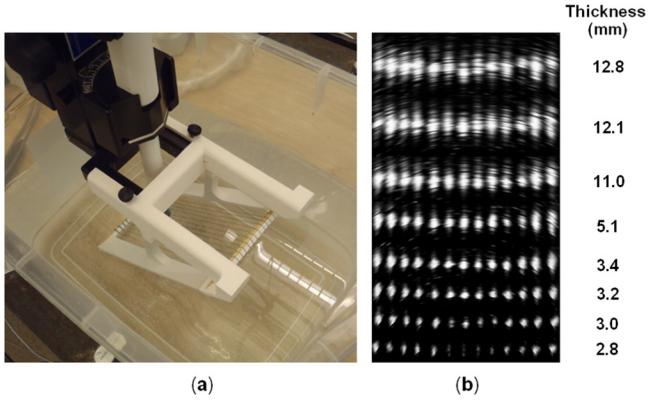

FIG. 8. (a) Beam profiling experimental setup. The TRUS probe and Wire-Bridge phantom are submerged in a glycerol–water bath. (b) Examples of beamwidth artifacts and their approximate height (thickness) over different depths of the TRUS images, frequency = 6 MHz, gain = 50%, dynamic range = 50 dB, and power = −4.

of thin, parallel, and low-intensity bands appear on both sides of the main lobe artifacts after side lobes intersect with the wires, as shown in Fig. 8(b).

III. EXPERIMENTS AND RESULTS

III.A. TRUS beamwidth measurement

Using the Wire-Bridge phantom, we measured the TRUS elevation beamwidth at different axial depths from the TRUS transducer. TRUS images were acquired with 6 MHz of central frequency, at 90 mm of imaging depth, 50 dB of dynamic range, and different gain settings (0%, 50%, and 100%).

Figure 8(b) illustrates a few examples of these measurements over several depths of the imaging region. The bright wire reflections in the TRUS images along with their surrounding lower-intensity side lobe artifacts (if present) were manually segmented by selecting multiple points and taking average of the measurements from the boundaries of the artifacts. A plot of linear interpolation of the TRUS elevation beamwidth versus vertical distance to the probe transducer (beam pattern/profile) are presented for a total of two lateral positions of wire reflections corresponding to the grid template holes in the TRUS images, as shown in Fig. 10. The TRUS beam pattern for each lateral locations of the images corresponding to the grid template holes were considered to find the relationship between the needle localization offsets and the beam pattern. The measurements cover the axial depths from 10 to 80 mm from the TRUS transducer face to examine the beamwidth profile with respect to the axial depths of the imaging area. The horizontal measurements of the beamwidth will examine the lateral variance of the beam pattern along the transducer crystal arrays. In our experiments, the TRUS images were acquired at 6 MHz central frequency, one of the commonly used frequency settings in the brachytherapy practice. We have measured elevation beam profile and the corresponding needle-tip offset with respect to the template grid indices and at different imaging settings. Figure 9 shows a 3D plot of the beam profile versus template grid indices. Figure 10 shows an example of the relationship in 2D.

III.A.1. Elevation beamwidth with respect to imaging settings

The following observations are made when comparing the elevation beamwidth with respect to TRUS imaging settings:

- The elevation beam profile provides important information regarding the quality and accuracy of the TRUS images at different vertical distances to the transducer. Looking at a TRUS image, we know that the rectum is located within 5–10 mm, the peripheral zone of the prostate (where 70%–80% of the cancer is located[25,26]) is within 10–28 mm, the urethra is within 28–40 mm, and the transitional zone of the prostate (where 10%–20% of the cancer is located[25,26]) is within 45–65 mm anterolateral to central gland from TRUS interface. Therefore, the quality of the TRUS images is much more vulnerable in the areas where most of the cancer is present and hence the highest accuracy is needed.
- The beam in the elevation direction had much smaller beamwidth when the gain was set to minimum as shown in Figs. 9 and 10. The beamwidth increased rapidly when the gain was increased to 50% and 100%. This rapid change was due to the increase in side lobe energies when gain was set to a higher value.
- There were three readings taken at each grid locations from the TRUS images of the profiling phantom. The TRUS beamwidth was measured to be 2.1 ± 0.4 mm at a distance of 13–15 mm to the transducer face when gain = 0% and remained low up to 3.3 ± 0.6 mm at the distance of 75–78 mm to the transducer. This value was 3.3 ± 0.6 mm and 5.5 ± 1.0 mm when gain = 50% and 100%, respectively, close to the transducer (13–15 mm) and increased up to 12.3 ± 1.8 mm and 15.7 ± 1.5 mm farther from the transducer (75–78 mm).

III.A.2. Elevation beamwidth with respect to the lateral positions of the template grid

The beam for all the lateral positions of the TRUS beam follows almost the same pattern. When gain is set to 50% or 100%, the effects of side lobe energies increase and there will be low-intensity echoes generated after these energies intersect with wires [shown in Fig. 8(b)]. Hence, the TRUS beamwidth increased constantly with larger values than when gain = 0% as shown in the beam profile measurement of Figs. 9 and 10.

III.B. Needle tip localization analysis

Observing the needle tip localization plots, the following results can be reported:

- According to Figs. 9 and 10, when gain = 50% or 100%, the needle offset graphs are absolutely increasing, which indicates that the TRUS beamwidth increases as the axial depth increases. This increase in the beamwidth is due to the

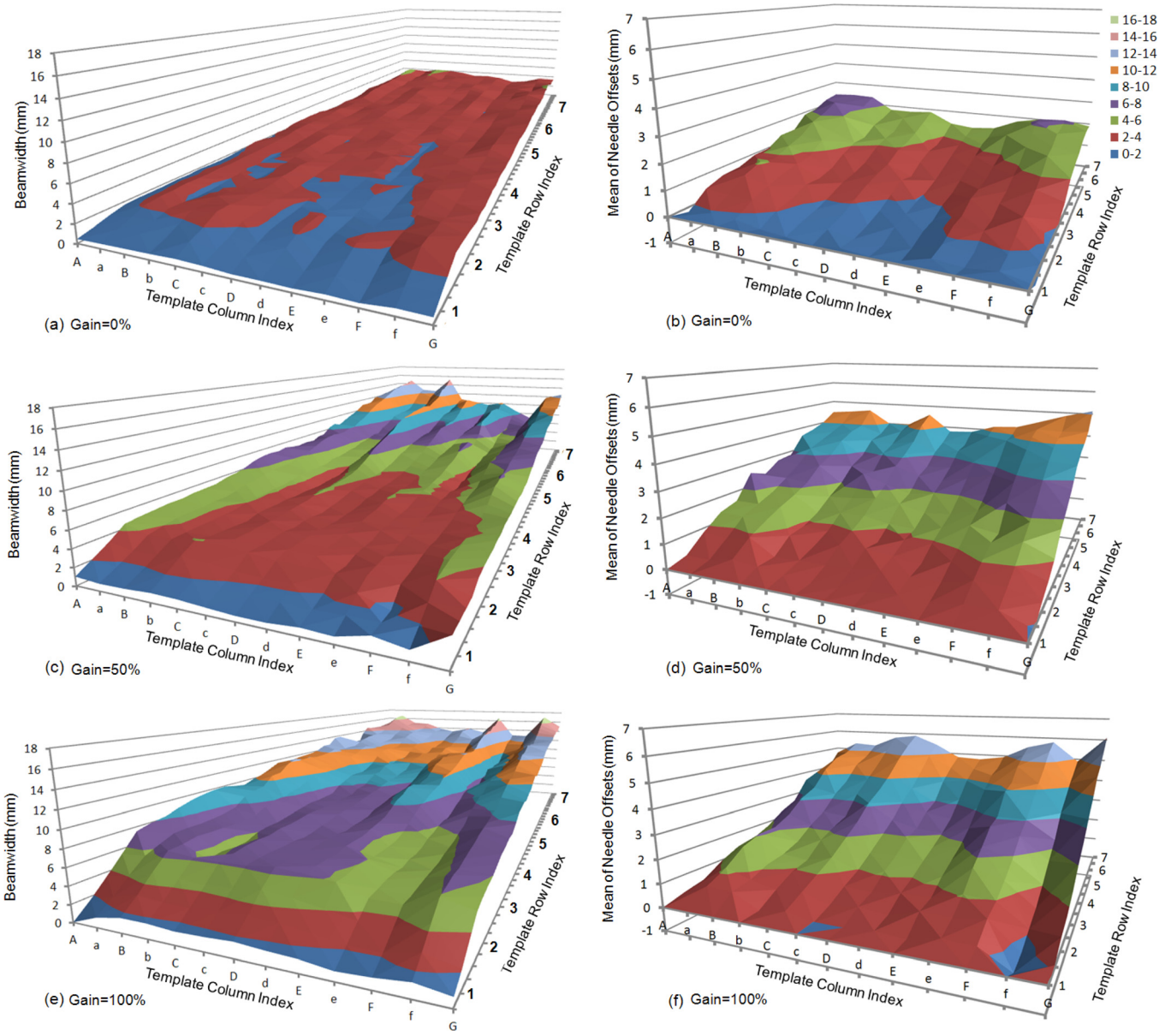

FIG. 9. (a)-(e) 3D surface plot of the elevation beamwidth profile with respect to the grid indices of the brachytherapy template at gain = 0%, 50%, and 100%, respectively; (b)-(f) the corresponding needle tip offsets at the same imaging setting.

increase in the main lobe thickness and the directed side lobe energies which diverge farther from the transducer. The needle insertion error is minimum close to the transducer since the side lobe energies are not far apart from the main beam energy and the needle tip intersects to the side lobes when they are closer to the actual main beam. The beam profile pattern also agrees with this finding.

- According to the beam profile graphs, when gain is turned high, the TRUS beamwidth increases at least two times more than the needle offset values. This could be explained using the TRUS beamwidth relationship equation introduced in Sec. II C and Fig. 4(b).
- As explained before, when a highly reflective material is intersected with the off-axis side lobes, the returning echoes are wrongly placed within the main TRUS beam as if the object is intersected with the main beam.[10] Therefore, during needle insertion, the needle tips are first intersected with the side lobe energies and the first echo reflections appear as if the needles are intersected with the main TRUS beam. This clearly indicates that the presence of both the main and side lobe beams has large effects on localizing needle tips in the TRUS images. On the other hand, when gain = 0%, side lobe energies are minimized or diminished and the needle offsets are less than zero near the transducer. This means that the beam converges up to a focal zone (around 26 mm from the transducer) where the beam thickness is minimum (around 1.5 mm). The beam thickness diverges quickly right after the focal zone to 4 mm at 78 mm axial distance to the transducer surface. This indicates that the TRUS beam thickness is much smaller when gain is set to zero than the case where gain is set to be high. Hence,

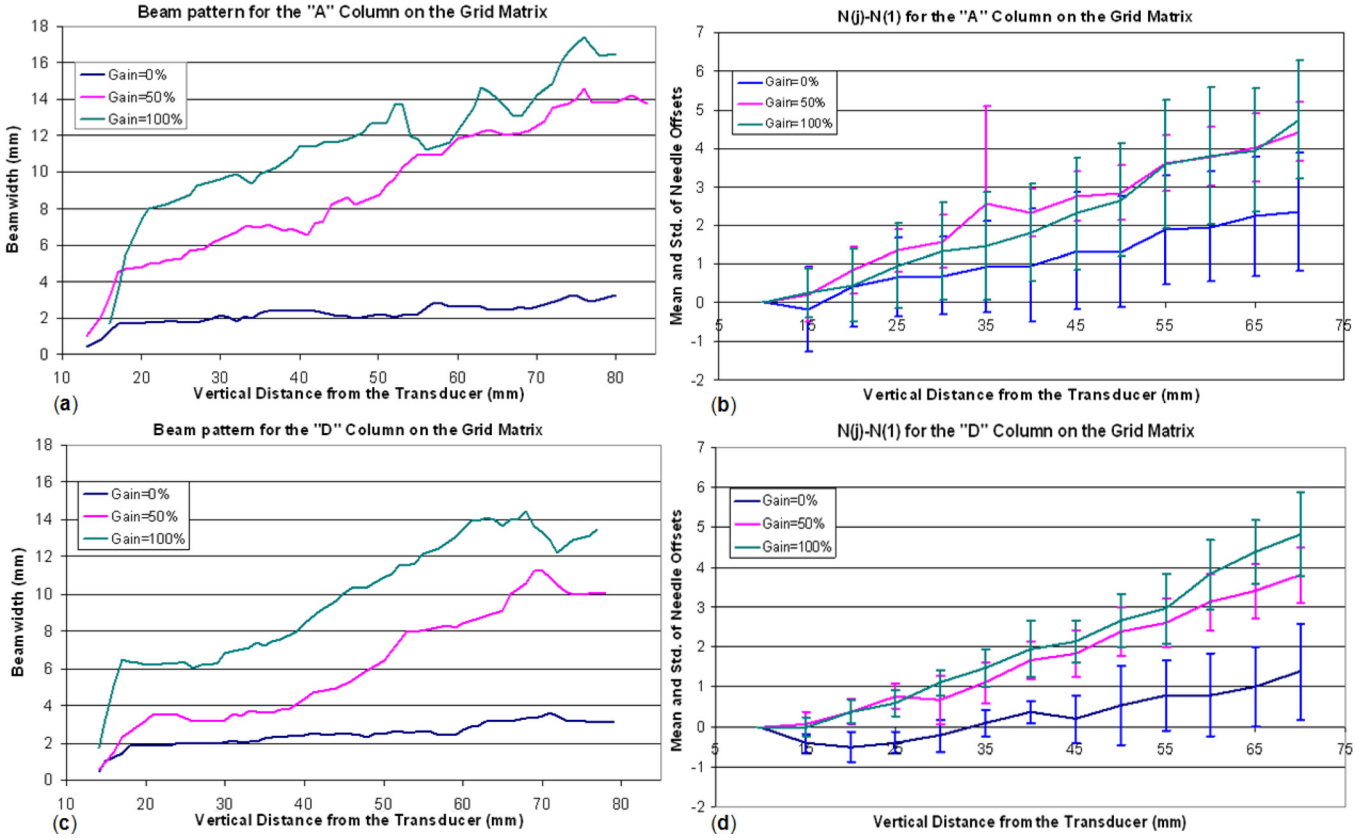

FIG. 10. (a) and (c) The TRUS elevation beamwidth profile at the template columns, A and D, with the dynamic range set to 50 dB and power at − 4. (b) and (d) The corresponding measurement of $N(j) - N(1)$ at lateral positions A and D for different gain, dynamic range, and power settings.

the amount of localization error decreases when gain is turned down.

- Looking at the needle offset diagrams at gain = 0%, when the needles are inserted at a location laterally farthest from the center of grid template (labeled with "D" on the template), needle offsets are greater than when close to the center.
- The maximum needle offset starts from approximately 2.3 mm at 70 mm distance from the reference needle and decreases to 1.3 mm as we move laterally toward the central portion of the grid template. The offset values start increasing as we move laterally toward the other side of the grid template (labeled as "G").
- The over all offset values laterally located away from the central portion of the grid template is also proportionally greater than the offset values captured along the central portion. This result indicates that the localization errors are higher when considering the holes located farther away from the center of the grid template and we will get more accurate localizations along the central portion of the grid.
- In addition, the TRUS beam is narrower along the grid central holes. When gain = 0%, the offset values within the first 30–35 mm from the reference needle are negative indicating that the beam was narrower with respect to the reference needle (as shown in Fig. 10). Therefore, localization errors are minimal as we move laterally toward the central portion of the grid template and when inserting needles axially within 40 mm distance to the TRUS transducer.

III.C. Comparison between beam profile and needle tip profile

As explained before, side lobes consist of multiple low-intensity off-axis beams that produce image artifacts around the main TRUS lobe.[6,10,11] When the gain is set to high, the energy assigned to the TRUS beams (main and side lobes) increase and hence their effects on TRUS images increase. These effects include images with higher intensities, noise levels, and more main and side lobe artifacts. Comparing the elevation beamwidth and needle tip measurement profiles, we can make the following points:

- When gain = 0%, the amount of energies assigned to main and side lobes are minimum, hence the artifacts caused by high energy beams are diminished or minimized.
- When gain = 50% or 100%, energies assigned to the TRUS beam increases and there will be more energies assigned to the side lobe beams. Hence, side lobe artifacts may be generated when these energies intersect with any object in the imaging medium. The higher the gain, the higher the amount of artifacts would be in the TRUS images.
- Similarly, when gain is set to be high, the main beam energy increases as well and the reflected echoes from the medium would have higher energies. Therefore, almost all the reflected echoes receive to the TRUS transducer and there will be a wider bright artifact (comparing to lower gain setting) appearing on the TRUS slices.

III.D. Side lobe extraction

Since the amount of side lobe energies are much less than the main lobe energy, there is a sudden drop in the pixel intensities between every parallel side lobe artifacts. Hence, this indicates the presence of multiple oriented side lobe energies around the main lobe energy, as explained before in Fig. 4.

IV. DISCUSSION

The fact that the TRUS focal zone is located close to the transducer essentially suggests that the TRUS device would provide the best elevational resolution within the focused beam region. In addition, the measured beam profiles and the needle offsets represent error maps in the TRUS images for different lateral distances of the beam. The calculated error maps could be used to improve brachytherapy applications by considering the likelihood of position errors on the TRUS data which are otherwise ignored or treated uniformly in the current practice.

In this research work, we did not consider the observer uncertainty of the measurements in needle tip and beam profiling experiments. However, this could be relevant to take the intra- or interobserver uncertainty of the operator into consideration when measuring the needle tip profiles in a future work.

Electronically set focal zones or focal lengths did not have any influence on the beam profile pattern and the thickness of the beam artifacts on the TRUS images. Electronic focusing can only improve the quality of the image slices along the lateral axis of the image plane. Focusing along the beam elevation plane is achieved mechanically.[6,12,27] In mechanical focusing, US beams are passed through an acoustic lens which works in the same manner as optical lens or by curving the transducer crystals which bend the sound waves toward a specific point (focal point) in the tissue.[6]

The elevation beamwidth of a linear-array transducer should only vary with the axial depth due to the planar arrangement of crystals along a straight line, where the axial depth is the perpendicular distance to the crystal surface and remains a constant value laterally.

On the other hand, for a curvilinear transducer, the beamwidth should vary both axially and laterally, because the axial depth is defined as the distance to the center of the curved, practically circular arrangement of the crystals,[6] and therefore varies for each point along the lateral axis. We have observed this phenomenon in our experiments with the transverse transducer of the TRUS probe.

An advantage of our Wire-Bridge phantom design comparing to the TRUS-Bridge phantom[12] was using multiple inclined wires in place of the rubber membrane. The rubber membrane was not a very reliable material to examine the elevation resolution of the TRUS beam since there is a chance of bending its surface after several experiments. We must make sure that the inclined surface does not bend during the experiments, which introduces error in measuring the beam thickness. Using high tension fishing lines reduces bending of the wires in our experiments. This also enables us to place the wires at the same lateral positions as that of the grid template holes to measure the beam thickness for each lateral positions.

In addition, the thickness of the wires is much smaller (negligible) than the rubber membrane. Hence, the wire thickness does not have great influence on observing beam thickness reflections.

We used glycerol-based solution as our coupling medium to image both the Wire-Bridge phantom and needle reflections experiments to match the speed of sound in biological tissues (1540 m/s).

We observed that the orientation of the beveled needle tips is important in the location at which needle tips start appearing in the TRUS slices. The beveled needles should be inserted in such a way that its beveled surface is opposite to TRUS transducer face. According to the brachytherapy stepper position reading, other orientations of the beveled needle tip could cause up to 4 mm of error in the position of the tip on TRUS images (according to the digital encoder values of the brachytherapy stepper).

V. CONCLUSIONS

We presented a new device to measure the TRUS elevation beamwidth. The design is compatible with any commercial brachytherapy stepper, and the use of fishing lines with negligible thickness allows to accurately measure TRUS elevation beamwidth. A large number of TRUS images with different imaging parameters (gain, dynamic range, power) at 6 MHz central frequency were acquired using the phantom from various axial depths from the transducer. The elevation beamwidth was extracted manually and a plot of TRUS beamwidth versus distance to the transducer was presented for different imaging settings.

The TRUS intensity gain was found to be an important parameter because it may cause significant needle localization error along the elevation beam axis. We provided evidence to show that decreasing the TRUS gain would decrease the side lobe artifacts. When both the main and side lobe artifacts of the TRUS are present in the image, the object localization error is maximum. We also found that the localization error is the smallest laterally near the center of grid template and axially close to the transducer, hence, the most trusted region for imaging.

Our experimental results suggest reducing the gain of the TRUS would effectively reduce the energies assigned to the TRUS main and side lobe energies. This could effectively minimize the amount of needle localization error which is otherwise 0.5 mm (when close to the transducer) to 4 mm (when farther from the transducer) along the elevation axis of the TRUS beam. This is obtained by finding the pairwise differences between every two axial locations of the needle offset profiles corresponding to gain = 50% or 100% and gain = 0% setting.

ACKNOWLEDGMENTS

This work was funded by the Natural Sciences and Engineering Research Council of Canada under the Idea to Innovation program. Gabor Fichtinger was supported as Cancer

Care Ontario Research Chair. Thomas Kuiran Chen was also the recipient of 2010-2011 MITACS Accelerate Ph.D. Fellowship.

[a]Author to whom correspondence should be addressed. Electronic mail: mpeikari@cs.queensu.ca

[1]A. Jemal, R. Siegel, J. Xu, and E. Ward, "Cancer statistics," Ca-Cancer J. Clin. **60**, 260–277 (2010).
[2]S. Nag, D. Beyer, J. Friedland, P. Grimm, and R. Nath, "American brachytherapy society recommendations for transperineal permanent brachytherapy of the prostate cancer," Int. J. Radiat. Oncol., Biol., Phys. **44**, 789–799 (1999).
[3]P. Bownes and A. Flynn, "Prostate brachytherapy: A review of current practice," J. Radiother. Pract. **4**, 86–101 (2004).
[4]A. Goldstein and B. L. Madrazo, "Slice thickness artifacts in gray-scale ultrasound," J. Clin. Ultrasound **9**, 365–375 (1981).
[5]G. Wan, Z. Wei, L. Gardi, D. B. Downey, and A. Fenster, "Brachytherapy needle deflection evaluation and correction," Med. Phys. **32**, 902–909 (2005).
[6]W. R. Hedrick, D. L. Hykes, and D. E. Starchman, *Ultrasound Physics and Instrumentation*, 2nd ed. (Elsevier, Mosby, Missouri, 2004).
[7]W. R. Hendee and E. R. Ritenour, *Medical Imaging Physics*, 4th ed. (John Wiley and Sons, Inc., New York, 2002).
[8]P. Hoskins, K. Martin, and A. Thrush, *Diagnostic Ultrasound, Physics and Equipment*, 2nd ed. (Cambridge University Press, Cambridge, UK, 2010).
[9]A. Thrush and T. Hartshrone, *Peripheral Vascular Ultrasound* (Elsevier, Philadelphia, 2005).
[10]F. C. Liang and A. B. Kurtz, "The importance of ultrasonic side-lobe artifacts," Radiology **145**, 763–768 (1982).
[11]M. K. Feldman, S. Katyal, and M. S. Blackwood, "US artifacts," Radiographics **29**, 1179–1189 (2009).
[12]M. Peikari, T. K. Chen, C. Burdette, and G. Fichtinger, "Section thickness profiling for brachytherapy ultrasound guidance," presented at SPIE Medical Imaging, Lake Buena Vista, FL, 2011.
[13]K. A. Scanlan, "Sonographic artifacts and their origins," Am. J. Roentgenol. **156**, 1267–1272 (1991).
[14]B. Richard, "Test object for measurement of section thickness at ultrasound," Radiology **221**, 279–282 (1999).
[15]M. L. Skolnick, "Estimation of beam width in the elevation (section thickness) plane," Radiology **108**, 286–288 (1991).
[16]P. Y. Barthez, R. Leveille, and P. V. Scrivani, "Side lobes and grating lobes artifacts in ultrasound imaging," Radiol. Ultrasound **38**, 387–393 (1997).
[17]J. F. Synnevag, A. Austeng, and S. Holm, "Adoptive beamforming applied to medical ultrasound imaging," IEEE Trans. Ultrason. Ferroelectr. Freq. Control **54**(8), 1606–1613 (2007).
[18]J. F. Synnevag and A. Austeng, "Minimum variance adaptive beamforming applied to medical ultrasound imaging," *Proc. IEEE Ultrason. Symp.* (IEEE-INST Electronical Electronic Engineers Inc., Piscataway, NJ, 2005), pp. 1199–1202.
[19]B. Mohammadzadeh Asl, and A. Mahloojifar, "Eigenspace-based minimum variance beamforming applied to medical ultrasound imaging," IEEE Trans. Ultrason. Ferroelectr. Freq. Control **57**(11), 2381–2390 (2010).
[20]J. A. Mann and W. F. Walker, "A constrained adaptive beamformer for medical ultrasound: Initial results," Proc. IEEE Ultrason. Symp. **2**, 1807–1810 (2002).
[21]Z. Wang, J. Li, and R. Wu, "Time-delay- and timereversal-based robust Capon beamformers for ultrasound imaging," IEEE Trans. Med. Imaging **24**, 1308–1322 (2005).
[22]F. A. Siebert *et al.*, "Imaging of implant needles for real-time HDR-brachytherapy prostate treatment using biplane ultrasound transducers," Med. Phys. **36**, 3406–3412 (2009).
[23]M. Peikari, T. K. Chen, A. Lasso, T. Heffter, and G. Fichtinger, "Effects of ultrasound section-thickness on brachytherapy needle tip localization error," in MICCAI 2011, LNCS 6891, edited by G. Fichtinger, A. Martel, and T. Peters (Springer-Verlag, Berlin, 2011), pp. 297–304.
[24]J. Bax, D. Smith, L. Bartha, J. Montreuil, S. Sherebrin, L. Gardi, C. Edirisinghe, and A. Fenster, "A compact mechatronic system for 3D ultrasound guided prostate interventions," Phys. Med. **38**, 1055–1069 (2011).
[25]F. S. vom Saal, C. E. Finch, and J. F. Nelson, *The Physiology of Reproduction*, 2nd ed. (Raven, New York, 1994), Chap. 61.
[26]M. Wirth, J. E. Altwein, B. Schmitz-Drager, and S. Kuptz, *Molecular Biology of Prostate Cancer* (de Gruyter, New York, 1998), Chap. 2.
[27]T. K. Chen, A. D. Thurston, M. H. Moghari, R. E. Ellis, and P. Abolmaesumi, "A real-time ultrasound calibration system with automatic accuracy control and incorporation of ultrasound section thickness," presented at SPIE Medical Imaging, 2008.